Adaptive kinetic Monte Carlo for first-principles accelerated dynamics

Lijun Xu and Graeme Henkelman[a)]
Department of Chemistry and Biochemistry, University of Texas at Austin, Austin, Texas 78712-0165, USA

(Received 11 May 2008; accepted 5 August 2008; published online 16 September 2008)

The adaptive kinetic Monte Carlo method uses minimum-mode following saddle point searches and harmonic transition state theory to model rare-event, state-to-state dynamics in chemical and material systems. The dynamical events can be complex, involve many atoms, and are not constrained to a grid—relaxing many of the limitations of regular kinetic Monte Carlo. By focusing on low energy processes and asserting a minimum probability of finding any saddle, a confidence level is used to describe the completeness of the calculated event table for each state visited. This confidence level provides a dynamic criterion to decide when sufficient saddle point searches have been completed. The method has been made efficient enough to work with forces and energies from density functional theory calculations. Finding saddle points in parallel reduces the simulation time when many computers are available. Even more important is the recycling of calculated reaction mechanisms from previous states along the dynamics. For systems with localized reactions, the work required to update the event table from state to state does not increase with system size. When the reaction barriers are high with respect to the thermal energy, first-principles simulations over long time scales are possible. © *2008 American Institute of Physics*. [DOI: 10.1063/1.2976010]

I. INTRODUCTION

Classical molecular dynamics simulations are limited by the time scales that can be accessed. An appropriate time step for atomic systems is on the order of a femtosecond, so that long trajectories are limited to nano- or microseconds. If such trajectories are integrated using forces from costly first-principles calculations, the accessible time scale is further reduced to picoseconds. This leaves a gap of several orders of magnitude between what can be simulated directly with classical dynamics and the human time scale of seconds or minutes. Most thermally activated chemical reactions take place on this longer experimental time scale, so there is a need for theoretical methods to model these important rare-event dynamics.

A. Accelerated dynamics

There are several approaches to bridging the time scale gap. Most progress has been made for systems in which the dynamics are governed by rare events between states on the potential energy surface. In these systems, statistical mechanics can be used to determine reaction rates so that the correct state-to-state dynamics can be calculated without having to model fast vibrational motion. Voter, in particular, made significant advances in this field by developing a number of accelerated dynamics methods.[1] These methods use a variety of approaches to speed up the rate of escape from each state visited in the dynamics. Parallel replica dynamics provides a linear acceleration with the number of replicas by running multiple trajectories in a state and accepting the first escape.[2] More acceleration is possible with hyperdynamics, which uses a bias potential to raise potential minima while leaving transition state regions unaltered,[3] and temperature accelerated dynamics,[4] which increases the simulation temperature to discover possible escape pathways. A strength of these methods is that the approximations are well controlled, so that conservative simulations recover the true dynamics. Additional work, however, is needed to reduce the computational overhead for systems that require the accuracy of density functional theory (DFT) to evaluate forces between atoms. The acceleration approach presented here will focus on such systems; with less control over the uncertainties but also with a lower computational overhead, it is possible to model long time scale dynamics from first principles.

B. Kinetic Monte Carlo

A popular method for modeling state-to-state dynamics is kinetic Monte Carlo (KMC).[5,6] If all kinetic events that are available to the system during the dynamics are known, as well as their rates, KMC can be used to determine a statistically correct sequence of events and time scale for the dynamics. In the context of atomic simulations governed by rare events, the reaction mechanisms and rates can be determined from a potential energy landscape using transition state theory (TST).[7] KMC is very efficient, allowing for the simulation of many millions of events with modest computational work. It is limited, however, in the range of systems that can be simulated. The most severe limitation is that all reaction mechanisms need to be identified at the outset of the simulation. To limit this set of possible mechanisms, events are generally described as the local movement of one or a few atoms. Complex and long-range mechanisms, as well as reactions with rates that are sensitive to their environment, are not generally allowed in a KMC database because the number of such events grows exponentially with their extent.

[a)]Electronic mail: henkelman@mail.utexas.edu.

There has been some work to characterize environment-dependent rates, but it remains to be seen how general and accurate these approaches are.[8–10] Another limitation of KMC is that the geometry of states must be matched to a table of possible reaction events. The most common solution to this matching problem is to restrict the simulation to a grid on which all configurations are described.

C. Adaptive kinetic Monte Carlo

Many of the limitations of KMC are relaxed in the adaptive KMC (aKMC) approach.[11] This method is very similar to KMC with one important exception: the reaction mechanisms available to the system are found during the simulation instead of determined *a priori*. In aKMC, the dynamics can take the system into unexpected configurations via complex reaction mechanisms that could not be included in a standard KMC event catalog.[12] The method is described as "adaptive" KMC because the list of possible events is not fixed—it adapts to the simulation environment during the dynamics. Another strength of aKMC is that there is no need to constrain the simulation to a grid or to define processes locally in terms of a few atoms.

The benefits of aKMC come with a high computational cost as compared to the regular KMC. From each new state visited, all relevant kinetic events must be found. For systems in which harmonic transition state theory[13,14] (hTST) provides sufficiently accurate reaction rates, finding all kinetic events is equivalent to finding all first-order saddle points leading from the current state to any new state. This can be done with a "min-mode" following algorithm,[15–17] which follows the lowest curvature mode from within a potential basin up to a nearby saddle point. Once a saddle has been found, the rate of the corresponding event is calculated as

$$k^{\mathrm{hTST}} = \frac{\prod_{i=1}^{3N} \nu_i^{\mathrm{init}}}{\prod_{i=1}^{3N-1} \nu_i^{\ddagger}} e^{-(E^{\ddagger}-E^{\mathrm{init}})/k_B T}, \tag{1}$$

where ν_i^{init} and $\nu_i^{\ddagger}$ are the ith stable normal-mode frequency at the initial and saddle point states, respectively, N is the number of particles moving in the transition, $E^{\ddagger}$ is the saddle point energy, and E^{init} is the energy of the initial state. The reaction mechanisms and rates are put in an event table and the KMC algorithm advances the simulation to the next state.

Since the aKMC method is based on hTST, the important dynamical events must be characterized by saddle points on the potential energy landscape. The method is not expected to work for systems with entropic bottlenecks or ubiquitous low barriers.

D. First-principles dynamics

Calculating the dynamics of a system from first principles or DFT is very challenging because of the high computational cost of calculating the force and energy. One way forward is to use DFT to calculate reaction rates and use these in a KMC simulation; there are many examples of this in the catalysis and surface dynamics literature.[18–21] Although these DFT calculations typically improve the accuracy of reaction rates as compared to those found with empirical potentials, this approach still suffers from all the limitations of KMC: only a small number of short-range reaction events can be modeled by mapping them onto a grid.

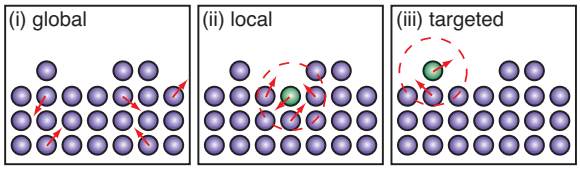

FIG. 1. (Color) Displacement algorithms used to initiate saddle point searches: (i) Displace all atoms, (ii) displace atoms around a central (green) atom, and (iii) displace atoms around a targeted central atom, in this case an undercoordinated surface atom. (Blue circles represent atoms in a box from a side view.)

In this work, we describe several improvements to the aKMC method to produce a method that is efficient enough to use directly with DFT. Specifically, we introduce a confidence parameter that determines the accuracy of the simulation, reaction rates are recycled from state to state, and new saddle point searches are done only in local regions where events occur. The combination of these improvements results in a method that scales well with system size and is efficient enough to model long time surface dynamics of metals on oxides from first principles.

II. METHODOLOGY

In this section, we briefly describe aKMC,[11] highlighting the changes that improve the accuracy and efficiency of the method.

A. Saddle point searches

An aKMC simulation starts from an initial minimum configuration. From this state and all distinct states visited in the dynamics, saddle point searches are used to find the processes available to the system. We have chosen to use the "dimer" min-mode following method[15] for these searches. Several improvements have been made to the dimer method since it was originally developed. These include the use of a forward-instead of a central-difference approximation,[22,23] a rotational force criterion to avoid unnecessarily accurate convergence of the lowest mode,[22,23] a large finite-difference rotation to improve stability with noisy *ab initio* forces,[23] the limited memory Broyden–Fletcher–Goldfarb–Shanno optimizer,[24] and internal coordinates for improved convergence.[25] With these advances, saddle points can be found from a local minimum in a few hundreds of force evaluations—not significantly more than a minimization.

Dimer searches are initiated near a local minimum by displacing the system away from the minimum. The displacement algorithm and magnitude are important for controlling the efficiency of the searches and the variety of saddles found. Figure 1 illustrates three different approaches used. The first (i) is very general; all nonfrozen atoms are displaced by a normally distributed random amount. An attractive feature of this algorithm is that there is some nonzero probability for all atoms to move to any other position in space and, in particular, to the neighborhood of any nearby saddle point. Using this general approach, the problem of

finding all saddle points reduces to a problem of sampling them. Of course, such an argument does not guarantee that all relevant saddles will be found efficiently, but it does address the concern that some important saddle could be entirely missed by the dimer searches. By viewing this as a sampling problem, we will take the usual approach of making sure that our sampled values (in this case, the event catalog) do not change with more searches.

If the modeler has some knowledge about the important kinetic events, this information can be used to focus the saddle point searches for higher efficiency. One such property of low energy reaction mechanisms in solid materials is that they involve a limited number of atoms in a local region of space. These events can be targeted by choosing a central atom in the system and displacing atoms in the local surrounding region to initiate a dimer search, as shown in Fig. 1(ii). Such local initial displacements do not constrain the events to the local region. For example, in aKMC simulations of diffusion on Al(100), displacements of single atoms still result in long-range cooperative diffusion events involving many atoms.[12]

One final displacement algorithm, illustrated in Fig. 1(iii), requires a selective choice of the locally displaced region. For surface diffusion and chemical reactions at surfaces, the undercoordinated surface atoms and any adsorbates on the surface are most likely to react. Focusing on these atoms improves the efficiency of the method. This approach should be used with care, however, to avoid user bias; combining targeted local searches with unbiased locally and globally initiated searches is a good strategy.

A second consideration is the magnitude of the initial displacement. Small displacements result in a narrow distribution of saddles near the initial minimum. Large displacements result in a wider variety of saddles, but also some searches that climb to prohibitively high energy and others that converge upon saddles that do not lead from the initial minimum. To check for this, minimizations are followed along both unstable directions from each saddle found, and if neither reaches the initial minimum, the saddle is disregarded. Ideally, the magnitude of the initial displacements should be chosen so as to optimize the variety of saddles found that lead from the initial minimum to a neighboring state.

B. How many saddle searches are enough?

For an accurate KMC simulation, all events with low energy saddle points and high rates must be included in the rate table. For aKMC, where these events are found with saddle point searches, we present a dynamic stopping criterion to decide when enough searches have completed. This criterion is based on the history of previous searches to evaluate the probability that an important saddle has been missed. There are two benefits from this: (i) such a criterion provides a level of confidence to the accuracy of the simulation, and (ii) states with only a small number of processes require only a small number of searches, whereas states with many new processes require more to satisfy the criterion. This criterion provides control over the cost and accuracy of the simulation.

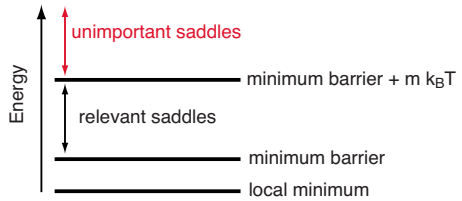

FIG. 2. (Color online) Reaction mechanisms with barriers within $m\ k_BT$ of the lowest saddle point energy are considered relevant. For a choice of $m=20$, the chance of a higher barrier process occurring in the dynamics is approximately e^{-20}.

The total number of saddles increases exponentially with the size of the system. Fortunately, most of these events have high barriers and are not important for constructing an accurate KMC event table. The window of relevant kinetic events has barriers within $m\ k_BT$ of the lowest barrier processes, for a suitably large m. This is illustrated in Fig. 2. Taking $m=20$ means that an event at the top of the window will be e^{-20} as likely to occur as the lower barrier event, assuming that the two have similar prefactors. Since $e^{-20}\approx 10^{-9}$ is small, the window of relevant saddles is still appropriate for events with prefactors that vary by several orders of magnitude. For systems with extremely different prefactors, a window of rates can be used instead.

To quantify a confidence level that all relevant saddles have been found, we start with a heuristic that all relevant saddle points are found with equal probability as we search for them. This is an ideal case that will allow for the derivation of a simple analytic convergence criterion—one that will be made more realistic in the next section. The confidence that a relevant saddle has not been missed for a state can then be written in terms of the following quantities: N_p, the number of relevant processes from the current state; N_s, the number of successful saddle searches finding a relevant (but possibly redundant) process; and N_f, the number of unique processes found. For each search, the probability of finding a new unique process is

$$P_f = \frac{N_p - N_f}{N_p} = \frac{dN_f}{dN_s}. \tag{2}$$

By taking a derivative, we are assuming that the discrete variables are large enough to be approximated as continuous variables. Integrating this differential equation gives the number of unique processes found after N_s searches,

$$N_f = N_p(1 - e^{-N_s/N_p}). \tag{3}$$

The probability that a relevant saddle will not be missed for a state is the fraction of unique saddles found. This is our ideal confidence parameter (ideal in the sense that we have based this on the ideal case of all saddles being found with equal probability),

$$C = \frac{N_f}{N_p} = (1 - e^{-N_s/N_p}). \tag{4}$$

A problem with this formula is that the total number of relevant saddles, N_p, must be known. For each new state visited N_p is unknown, but it can be determined from the saddle point searches. To do this, we introduce another quantity, N_r, the number of sequential searches that find relevant but redundant (nonunique) processes. For each of these searches, the probability of finding a new and unique saddle is P_f from Eq. (2). After N_r searches, one new and unique saddle is found, so that $N_r P_f = 1$ and therefore

$$\frac{1}{N_r} = P_f = e^{-N_s/N_p}, \tag{5}$$

assuming that P_f is constant for the N_r searches. The confidence that a saddle will not be missed in the event table can then be related to N_r by

$$C = \left(1 - \frac{1}{N_r}\right), \tag{6}$$

which is the main result of this section. It means that one can choose a confidence that an important saddle will not be missed in each KMC step. For example, a choice of $C = 95\%$ is set by running saddle point searches until $N_r = 20$ searches complete without finding a new, unique (and relevant) saddle point. Fewer total searches will be required for states with fewer relevant saddles than for states with many.

C. Confidence when saddles are hard to find

The heuristic that all saddles are found with equal probability describes the best-case scenario. The statistics of min-mode following calculations show that there is a significant variation in the probability in which saddles are found,[15] and this variability alters the confidence that an important saddle is not missed. To quantify the confidence when some saddles are hard to find, we use a parameter, α, which is the relative probability of finding the saddle that is least likely to be found as compared to the ideal case of the previous section, $1/N_p$. That is, the minimum probability of finding any one saddle is

$$P_{\min} = \frac{\alpha}{N_p}, \tag{7}$$

where $0 < \alpha \leqslant 1$. For $\alpha = 1$, we recover the ideal case of equal probabilities. In general there will be some nonuniform probability distribution of finding saddles with a minimum value $P_{\min}$. To derive a confidence parameter, we will take the worst-case scenario: that all saddles are found with this minimum probability, except one. For $\alpha < 1$, at least one saddle must have a probability greater than the average, $1/N_p$, since the probability of finding any of the N_p saddles is unity. The worst case is for one saddle to be found with the high probability,

$$P_{\max} = 1 - \alpha\left(\frac{N_p - 1}{N_p}\right). \tag{8}$$

The confidence parameter describes the probability of missing a saddle, so for $N_p \gg 1$ we can ignore this process since it will be found with a much higher probability than the others,

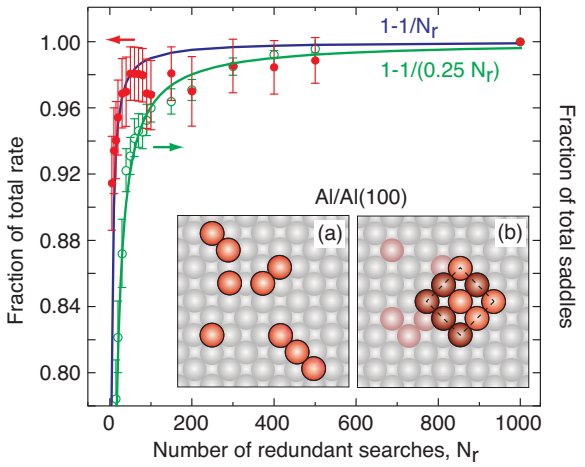

FIG. 3. (Color) Test of the aKMC confidence parameter for a 0.32 s dynamics simulation of (a) nine Al adatoms, which ripen into (b) a compact island on Al(100) at 135 K. The fraction of the total rate (red, left) and the relevant saddles found (green, right) follow the analytic confidence relations of Eq. (6) (blue, upper curve) and Eq. (14) with $\alpha = 0.25$ (green, lower curve).

$$\frac{P_{\max}}{P_{\min}} \sim \frac{N_p}{\alpha}. \tag{9}$$

Again, for large N_p where $N_p \sim N_p - 1$, the statistics of finding $N_p - 1$ saddles with probability $P_{\min}$ is the same as the equal-probability case discussed in the previous section, except that the probability of finding each saddle is reduced by the factor α. Following the same derivation, Eq. (2) becomes

$$P_f = \alpha\left(\frac{N_p - N_f}{N_p}\right) = \frac{dN_f}{dN_s}; \tag{10}$$

the number of unique saddles found, N_f, in terms of the number of searches, N_s, is

$$N_f = N_p(1 - e^{-\alpha N_s/N_p}); \tag{11}$$

and the confidence of not missing a saddle is

$$C = \frac{N_f}{N_p} = (1 - e^{-\alpha N_s/N_p}). \tag{12}$$

Using the number of redundant saddles, N_r, from the criterion $N_r P_f = 1$ yields

$$\frac{1}{N_r} = P_f = \alpha\left(1 - \frac{N_f}{N_p}\right) = \alpha e^{-\alpha N_s/N_p}, \tag{13}$$

and substituting into Eq. (12) gives a confidence,

$$C = \left(1 - \frac{1}{\alpha N_r}\right). \tag{14}$$

Taking $\alpha = 1$, which is the equal-probability case of the previous section, this confidence reduces to Eq. (6).

D. Testing the confidence parameter

To check the validity of this confidence parameter, we simulated the diffusion and ripening of Al adatoms on the surface of Al(100) with an embedded atom method potential.[26] The simulation started with nine randomly deposited atoms on the surface, as shown in Fig. 3(a) and

ended after 0.3 s when a compact square island formed on the surface in the configuration shown in Fig. 3(b). Note that Al adatoms diffuse via an exchange mechanism on this surface[27] so that the adatoms in the initial configuration are not the same as those in the final state; the light red atoms in the substrate of Fig. 3(b) show the final location of the original adatoms.

These dynamics involved 47 310 transitions between 62 unique states. In this calculation, $N_r=1000$ redundant searches were used as a stopping criterion for each state. For an ideal value of $\alpha=1$, this corresponds to a confidence parameter of $C=99.9\%$ from Eq. (6). The actual measured probability of missing an important saddle (the confidence) was then tested by recalculating the set of relevant saddles at each state using different values of N_r. Two measures of accuracy were tested; the number of relevant saddles found and the cumulative rate of these processes as compared to the $N_r=1000$ calculation. Figure 3 shows how these two fractions approach unity as the number of redundant searches is increased. The fraction of the total rate follows the ideal $\alpha=1$ confidence from Eq. (6). The fraction of the number of saddles increases more slowly, following Eq. (14) with $\alpha=0.25$. The reason for this is that the dimer method finds low energy saddles with greater frequency than high energy saddles,[15] here by a factor of 4. The high energy saddles, however, are exponentially less important than the low energy saddles, so that the cumulative rate is a much better measure of convergence than the number of saddles. Although the ideal $\alpha=1$ case is a good approximation for this system, convergence tests should be run to estimate a conservative value for α, so that the confidence can be established for a choice of N_r using Eq. (14).

E. Recycling saddle points

We now have a way of finding all important saddle points leading away from a state to a specified confidence level. These reaction mechanisms and rates are used to build a KMC rate table so that an event can be selected with the appropriate probability and the system advanced to the final state of that chosen process. At this new state, a new event table is required. Instead of starting from scratch, the information of processes from the previous state (as well as other states and calculations) can be used to efficiently build the new event table. We describe this process as recycling saddle points.

Recycling saddle points from previous states is most important for systems with local processes in which a subset of atoms moves significantly and the structure of the rest of the system remains largely unchanged. Figure 4 is a cartoon of such a system with atoms moving on a surface. Seven hopping processes are illustrated and used to construct a rate table. Process 7 is selected in the KMC step. For the next KMC step, a new event table is required. Processes 1–5 are largely unaffected by the chosen process and can be recycled (updated) from the old to the new event table at minimal cost. Any events in the old table that were close to the chosen process (process 6) will be affected, leaving a hole in the event table. This hole will extend only as far as the range of

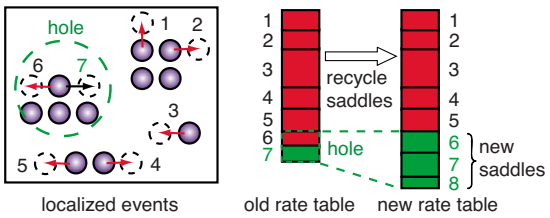

FIG. 4. (Color online) For systems with local events, the mechanism and rates of distant events can be recycled to build a new rate table very quickly. New searches are concentrated in the region around the chosen process, for which there is a hole in the rate table. Then, the cost of updating the rate table does not increase with system size.

the local processes, so that the work of filling it in the new table does not require new saddle searches across the entire system. For large systems, the number of searches required at each KMC step does not increase with system size. The efficiency improvements and favorable scaling with system size due to process recycling are demonstrated later.

First, we need to describe how processes are recycled from state to state. The ith process is defined by the coordinates of the initial state, $\vec{R}_i^{\text{init}}$, saddle point, $\vec{R}_i^{\text{sp}}$, and final state, $\vec{R}_i^{\text{final}}$. The normal mode at the saddle, $\hat{N}_i^{\text{sp}}$, is also known. Let an additional subscript j denote a particular atom, so that $\vec{R}_{i,j}^{\text{init}}$ is the coordinates of the jth atom of the initial minimum in the ith process. A KMC step is made by selecting one process, which we will denote with subscript $i=0$. The recycling of all other processes is then attempted by merging their saddle point configuration, $\vec{R}_i^{\text{sp}}$, with the final state of the chosen process, $\vec{R}_0^{\text{final}}$, which is the initial state of the next KMC step. This is done with a single distance parameter, dR, which is taken to be 0.2 Å in all of our calculations presented here. Atoms that move by more than dR in the chosen process are set in the final configuration of the chosen process. Atoms that move by less are placed in the configuration of the saddle of the recycled process. The coordinates of the recycled saddle, $\vec{R}_{i,j}^{\text{sp}_{\text{recyc}}}$, are taken to be

$$\vec{R}_{i,j}^{\text{sp}_{\text{recyc}}} = \begin{cases} \vec{R}_{i,j}^{\text{sp}} & \text{if } |\vec{R}_{0,j}^{\text{final}} - \vec{R}_{0,j}^{\text{init}}| < dR \\ \vec{R}_{0,j}^{\text{final}} & \text{if } |\vec{R}_{0,j}^{\text{final}} - \vec{R}_{0,j}^{\text{init}}| > dR, \end{cases} \tag{15}$$

and the negative mode is taken along the vector

$$\vec{N}_{i,j}^{\text{sp}_{\text{recyc}}} = \begin{cases} \hat{N}_{i,j}^{\text{sp}} & \text{if } |\vec{R}_{0,j}^{\text{final}} - \vec{R}_{0,j}^{\text{init}}| < dR \\ 0 & \text{if } |\vec{R}_{0,j}^{\text{final}} - \vec{R}_{0,j}^{\text{init}}| > dR. \end{cases} \tag{16}$$

From this approximate saddle point configuration and negative mode, a saddle point search is used to converge to a (hopefully) nearby saddle. If the recycled process is distant from the chosen process, the search converges very quickly. To the extent that the recycled and chosen processes overlap, the initial configuration can be unphysical and the search will fail. This indicates that the recycled process falls into the hole in the event table where fresh searches are required.

Figure 5 illustrates how three processes (b)–(d) are recycled given the chosen process (a) for a step in the aKMC dynamics of Al ripening on Al(100). The recycling of the other processes is done by taking their saddle point configuration and setting the position of any atoms that moved sig-

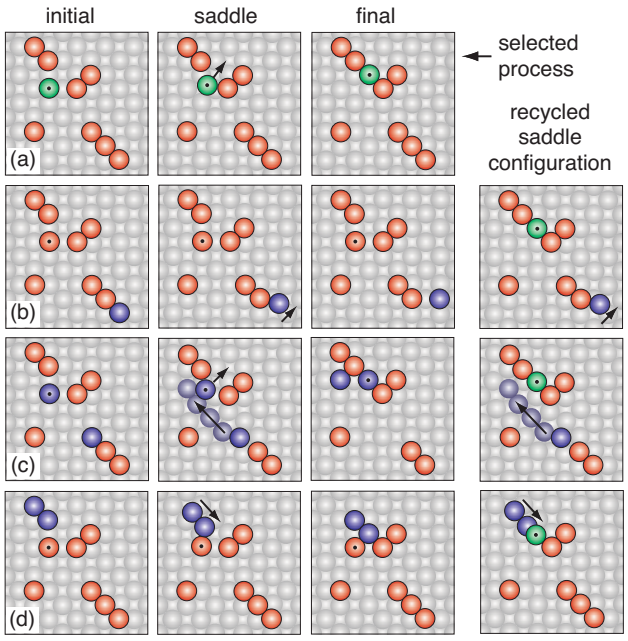

FIG. 5. (Color) Examples of recycling saddle points from a previous state for Al diffusion on Al(100). To recycle a saddle, atoms that move significantly in the chosen process (a) are identified. Here, the one atom that moved by more than $dR=0.2$ Å is marked with a (●). Then, in the saddle geometry of all other processes [(b), (c), and (d)], these moving atoms are set in their final-state positions of the chosen process.

nificantly in the chosen process (green, marked with a dot) to their position in the final state of the chosen process. For a distant process (b) the recycled saddle is a good initial guess and converges to a true saddle with minimal cost. Process (c) is in close proximity to (a), but the recycling rules result in a fair initial guess of a saddle that converges to a long-range exchange event in the new state. Processes (d) and (a) are too close so that the recycled initial saddle geometry is high in energy. Processes this close to (a) need to be found with new saddle searches.

Large systems with local processes benefit a lot from this recycling approach. Figure 6 shows how the computational cost, evaluated in terms of the number of force evaluations, is reduced when saddles are recycled. A single evaluation of the force is for all atom in the system. In this test, a two-step simulation of Al diffusion on Al(100) is done for a range of confidence parameters, $C=1-1/(\alpha N_r)$, taking $\alpha=1$. The initial configuration is shown in Fig. 3(a). The cost is measured only for the second KMC step. With saddle recycling, all the

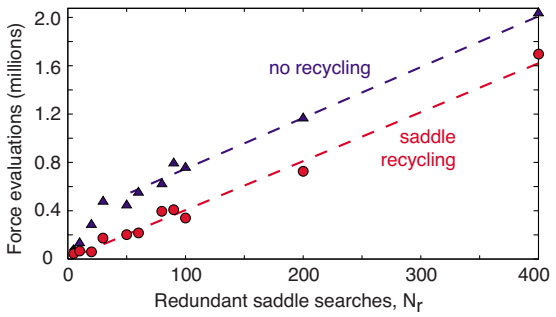

FIG. 6. (Color online) The computational cost for a KMC step is significantly reduced by recycling saddles from the previous step.

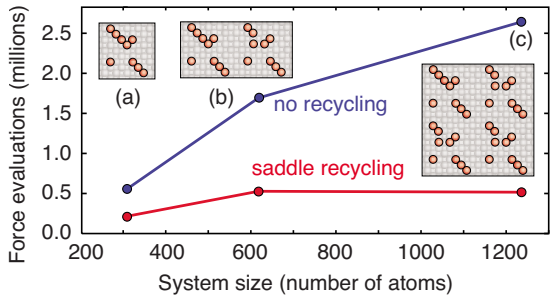

FIG. 7. (Color online) For a system with local processes, recycling saddles from one state to the next results in a computational effort (measured by the number of force evaluations) that does not increase with system size. The insets show how the smallest Al/Al(100) system was expanded to make larger systems for this calculation.

processes found in the first step are used to help build the rate table for the second step. Without recycling, the rate table is built from scratch. There is a significant improvement in efficiency when recycling is used even for this modest system size. The biggest gain is for confidence values of 90%–99% ($N_r=10-100$). At higher accuracy, the cost of both calculations is dominated by finding N_r redundant saddles after the event table is found, which explains the parallel linear trend at high values of N_r.

This same model system was used to test how saddle recycling changes the scaling of the aKMC computational cost with system size. Figure 7 shows three Al substrates with 309, 618, and 1236 atoms, formed by making copies of the smallest system. The Al/Al(100) test was used to compare the cost of building a rate table with and without recycling, using a stopping criterion of $N_r=60$ (a confidence $C=98\%$ with $\alpha=1$). For the smallest system, recycling halves the number of required force evaluations. For larger systems, there is a greater fraction of saddles that can be recycled, so the benefit of recycling is even higher. If the range of the processes is smaller than the system size, the cost of updating the rate table does not increase with system size. This excellent scaling is the most important reason to use process recycling in aKMC simulations.

A couple of comments should be made about this scaling result. First, unless the force evaluation can be localized, the cost of each force evaluation will increase with system size so that the actual computational effort will also increase. Second, if one system is compared to another system that is exactly twice as big and has twice the number of available processes, the amount of time simulated in each KMC step will be cut in half, so that twice as many KMC steps are needed to reach the same simulation time as that in the small system. The recycling of processes improves the scaling of the cost to build the KMC event table; the scaling of the KMC dynamics for systems with localized processes can also be made efficient but in different ways.[28,29]

F. States connected by low barriers

KMC is efficient when there is a clear separation of time scales between vibrational motion and the state-to-state dynamics. Fast rates between states reduce the efficiency of KMC. For dynamics at surfaces, it is not unusual to encoun-

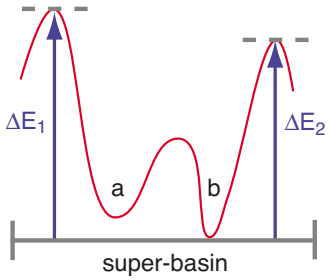

FIG. 8. (Color online) A superbasin is composed of states (a and b) that are connected by much lower barriers than the barriers to leave the superbasin ($\Delta E_1, \Delta E_2$). To avoid a large number of oscillations between states in the superbasin, they are taken to be a single state in local equilibrium.

ter fast diffusion processes on the time scale of pico- or nanoseconds in a simulation for which there are also important events on the micro- or millisecond time scale. Even though each KMC step requires a small computational effort, it can be prohibitively expensive to simulate millions or billions of fast events. In the Al/Al(100) surface ripening simulations, for example, fast processes such as trimer rotation and edge running are encountered frequently and are costly to model explicitly at low temperatures.

In our simulations we avoid the explicit modeling of fast oscillation between pairs of neighboring states. Figure 8 illustrates two such states, a and b, separated by a lower barrier than those required to leave the two states. If the motion between a and b is rapid, equilibrium will be quickly reached so that the two states can be considered a single superbasin. A superbasin is detected in the following way. When a new state is reached, the rate of each event is compared to the total rate to leave the state, and a flag is set if the ratio is greater than a certain value. In our simulations, we set this ratio to 99.999%, indicating that the fastest event will be chosen with this high probability. If the fastest event is chosen in the KMC step, the same comparison is made in the new state. If each state has one dominant process leading to the other, they are marked as belonging to a superbasin. A new combined rate table is then constructed from all processes leading out of the superbasin. All barriers are taken with respect to the lower energy state, ΔE_1 and ΔE_2 in Fig. 8. If states a and b are visited in the subsequent dynamics, the combined rate table is used to make a KMC step from that superbasin. This approach can be extended to superbasins with more than two states. Reference 30 and the references therein have an in-depth discussion of this approach.

III. FIRST-PRINCIPLES AKMC DYNAMICS

DFT calculations are much more expensive than the empirical potential calculations described so far. With current computers, it is just becoming possible to combine DFT with aKMC to model rare-event dynamics. Both the efficiency improvements described and the fact that saddle searches are independent and can be calculated in parallel make the simulations possible. With many computers, even loosely coupled ones, the time required for each KMC step reduces to the time required to evaluate the rate of a single process.

To simplify the process of running many independent saddle point searches, we have developed a script that can run aKMC dynamics by automatically sending the calculations to a cluster of computers, a supercomputer, or distributed computing resources.[31] This script implements the methods described here using forces from the Vienna *Ab-initio* Software Package (VASP) DFT code.[32] A schematic of how the script works is illustrated in Fig. 9. The script keeps track of the aKMC dynamics calculation and, as needed, submits DFT jobs to the available computers via a queuing system. Automating this process is essential given the large number of calculations required for a dynamics simulation.

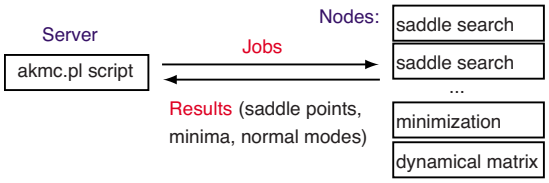

FIG. 9. (Color online) An aKMC script automatically submits calculations on a cluster of computers, restarts incomplete jobs, finds saddles and corresponding final states, collects kinetic processes and rate, and performs the KMC steps.

A. Pd cluster formation on MgO(100)

To demonstrate how the aKMC method can be used with DFT to calculate dynamics over long time scales, we have modeled the formation of a Pd cluster on the MgO(100) surface starting from four separated Pd adatoms. Not only is this a model system for heterogeneous catalysis,[33] but there is also some recent interest in a better understanding of these ripening dynamics.[21,34–37] It has been shown that Pd clusters form at defect sites, so we have put one Pd monomer initially at a F+ center oxygen vacancy site, where it is bound irreversibly at a simulation temperature of 300 K. From this initial configuration, the aKMC method is used to calculate a state-to-state dynamical trajectory. For this simulation, we used process recycling with $dR=0.2$ Å and $N_r=10$ sequential redundant saddle searches in each state (a confidence of $C=90\%$ for $\alpha=1$). Superbasin detection was used, but no such states were found in this simulation.

The MgO substrate was modeled by a two-layer slab with 36 atoms in each layer, with the atoms in the bottom layer held frozen at the bulk lattice positions. Convergence tests of Pd binding show that the two-layer model is sufficient since the MgO substrate is so rigid. The Perdew–Wang 91 generalized gradient functional[38] was used to model electronic exchange and correlation. Pseudopotentials of the Vanderbilt form[39] constructed within the projected augmented wave framework were used,[40] as implemented in VASP. A plane wave basis set with an energy cutoff of 251 eV and a Γ-point sampling of the Brillouin zone were found to be sufficient. Geometries were considered converged when the force dropped below 0.003 eV/Å on each atom. The rates of reaction were calculated with Eq. (1) using a standard prefactor of 10^{12} s^{-1}.

The Pd cluster formation dynamics, shown in Fig. 10, consists of ten aKMC steps between nine unique states (the state reached at 11 μs is repeated). On a time scale of microseconds, Pd hopping between O sites is activated, and a two-dimensional cluster forms. For these states, processes

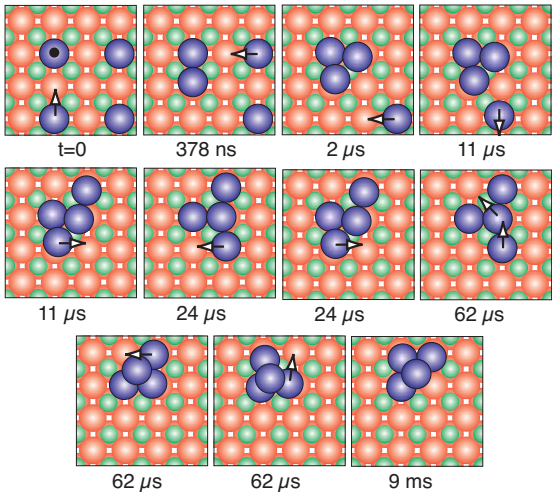

FIG. 10. (Color) The DFT-based aKMC simulation of a Pd tetramer formation at an O vacancy site (●) on the MgO(100) surface over a time scale of 9 ms at 300 K. [Circles: O (red), Mg (green), and Pd (purple)].

recycling offered a significant speedup because of the many equivalent hopping events available to each Pd monomer. At 62 μs an interesting low-energy concerted exchange takes place, resulting in a Pd atom being pushed up on top of other three to form a three-dimensional tetrahedron. In the following steps, the tetramer evolves through a few different conformations, reaching a time scale of milliseconds. Here, the tetramer is pinned at a defect, but in another work looking at Pd cluster diffusion on the MgO terrace, it was shown that this tetramer is the fastest diffusing species on the terrace and that it diffuses via a rolling mechanism.[35] The rapid formation and diffusion of three-dimensional clusters has been shown to be important for kinetic modeling of Pd growth on MgO(100).[21]

B. Ca oxidation at a MgO step

As a second test, we investigated the dynamics of Ca oxidation on MgO(100). Previous experimental studies have shown that Ca atoms bind to MgO(100), giving off an initial heat of adsorption of 4.2 eV, and that roughly 7% of the surface is covered with defects that (on average) bind Ca this strongly.[41] This is higher than the calculated binding of Ca to steps (2.3 eV) and kinks (3.9 eV).[42] The calculated kink-site binding is fairly close to the experimental binding, but a grown MgO crystal is unlikely to have 7% kink defects. The aKMC simulation, illustrated in Figs. 11 and 12, investigates a possible explanation for the high measured heat of adsorption. The MgO surface is made by oxidizing Mg in the presence of O_2 at high temperatures. If some of the O_2 remained on the surface after annealing, it could combine with deposited Ca, releasing the high energy of Ca oxidation. This was investigated with a DFT-aKMC dynamics simulation of a Ca atom next to an adsorbed O_2 molecule at a MgO(100) step edge. The details of the DFT calculations are similar to those described in the previous section and are discussed more fully in Ref. 42. The same value of $dR=0.2$ Å was used for process recycling and $N_r=10$ for the confidence level.

Figure 11 shows the wide range of kinetic events found by dimer min-mode following searches from this initial state.

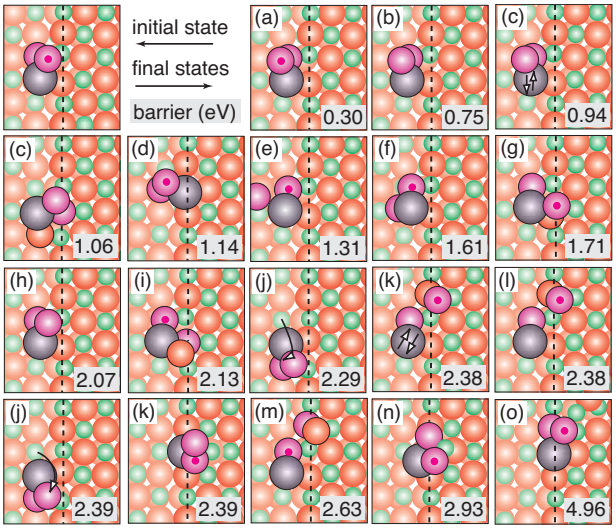

FIG. 11. (Color) Reaction mechanisms from an initial state with O_2 adsorbed next to a Ca atom at a step on the MgO(100) surface, found using DFT forces with dimer searches. (Red atoms are O from MgO, pink are O from O_2, green are Mg, gray are Ca, and the dashed line is the step edge. The pink dot is used to distinguish the O_2 atoms.)

The fastest processes involve simple O_2 libration [(a) and (b)]. Processes with higher barriers involve complex O_2 motion, replacing O atoms from the surface [(c) and (o)], or dissociation and recombination with surface-bound O [(g), (i), (k), (l), and (m)]. In the dynamics, shown in Fig. 12, O_2 is found to first librate and reach equilibrium between two low energy states at 1.5 ps. Since the libration rate is so much higher than any other event, these two states were considered a single superbasin, avoiding the explicit modeling of about 50 million trivial KMC steps. After 10 ms, the O_2 pushes out a surface O atom to form a peroxy species. The peroxy species then rapidly oscillates between two stable conformers before dissociating into lattice sites to form a small O–Ca–O step. If O_2 or step-bound peroxy species were present on the annealed MgO(100) surface, the oxidation of deposited Ca atoms could contribute to the high experimental heat of adsorption as compared to DFT.

IV. CONCLUSIONS

Two improvements have been made to the aKMC methodology for simulating dynamics over long time scales: (i) a

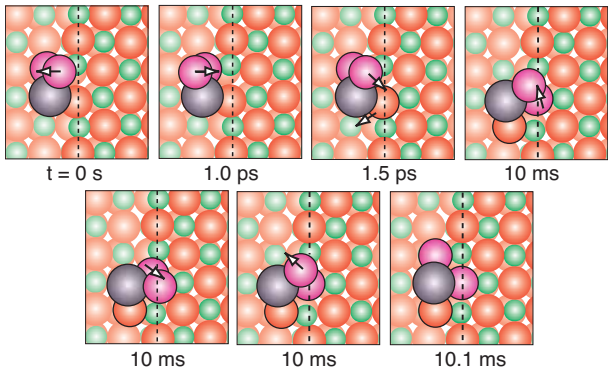

FIG. 12. (Color) DFT dynamics of Ca oxidation on the MgO(100) surface at 500 K.

confidence parameter has been introduced, which provides a dynamic criterion for deciding when to stop searching for saddles from each new state, and (ii) the recycling of saddles from state to state improves the efficiency and scaling of the method for systems with local processes. Also, our implementation of the method can make use of large parallel and distributed computing resources so that it is possible to calculate state-to-state, rare-event chemical dynamics at surfaces using forces and energies from DFT without having to anticipate the important reaction mechanisms.

ACKNOWLEDGMENTS

The authors are grateful for many helpful discussions with Hannes Jónsson, Arthur Voter, and Blas Uberuaga, who all contributed to developing these methods, and to Charles Campbell for suggesting the Ca oxidation calculations. This work was supported by the National Science Foundation CAREER Award No. CHE-0645497 and the Robert A. Welch Foundation under Grant No. F-1601. The authors are grateful for allocations of computing resources at the Molecular Science Computing Facility at the Pacific Northwest National Laboratory (Project No. EMSL-25428) and the Texas Advanced Computing Center. Finally, the authors thank John Griffin and all the other people who contributed computing time through the EON project.[43]

[1] A. F. Voter, F. Montalenti, and T. C. Germann, Annu. Rev. Mater. Res. **32**, 321 (2002).
[2] A. F. Voter, Phys. Rev. B **57**, R13985 (1998).
[3] A. F. Voter, Phys. Rev. Lett. **78**, 3908 (1997).
[4] M. R. Sørensen and A. F. Voter, J. Chem. Phys. **112**, 9599 (2000).
[5] A. B. Bortz, M. H. Kalos, and J. L. Lebowitz, J. Comput. Phys. **17**, 10 (1975).
[6] D. T. Gillespie, J. Comput. Phys. **22**, 403 (1976).
[7] A. F. Voter, Phys. Rev. B **34**, 6819 (1986).
[8] E. W. Hansen and M. Neurock, J. Catal. **196**, 241 (2000).
[9] O. S. Trushin, A. Karim, A. Kara, and T. S. Rahman, Phys. Rev. B **72**, 115401 (2005).
[10] K. Reuter and M. Scheffler, Phys. Rev. B **73**, 045433 (2006).
[11] G. Henkelman and H. Jónsson, J. Chem. Phys. **115**, 9657 (2001).
[12] G. Henkelman and H. Jónsson, Phys. Rev. Lett. **90**, 116101 (2003).
[13] C. Wert and C. Zener, Phys. Rev. **76**, 1169 (1949).
[14] G. H. Vineyard, J. Phys. Chem. Solids **3**, 121 (1957).
[15] G. Henkelman and H. Jónsson, J. Chem. Phys. **111**, 7010 (1999).
[16] L. J. Munro and D. J. Wales, Phys. Rev. B **59**, 3969 (1999).
[17] R. Malek and N. Mousseau, Phys. Rev. E **62**, 7723 (2000).
[18] K. Reuter, D. Frenkel, and M. Scheffler, Phys. Rev. Lett. **93**, 116105 (2004).
[19] D. Mei, Q. Ge, M. Neurock, L. Kieken, and J. Lerou, Mol. Phys. **102**, 361 (2004).
[20] K. Honkala, A. Hellman, I. N. Remediakis, A. Logadottir, A. Carlsson, S. Dahl, C. Christensen, and J. K. Nørskov, Science **307**, 555 (2005).
[21] L. Xu, C. T. Campbell, H. Jónsson, and G. Henkelman, Surf. Sci. **601**, 3133 (2007).
[22] R. A. Olsen, G. J. Kroes, G. Henkelman, A. Arnaldsson, and H. Jónsson, J. Chem. Phys. **121**, 9776 (2004).
[23] A. Heyden, A. T. Bell, and F. J. Keil, J. Chem. Phys. **123**, 224101 (2005).
[24] J. Nocedal, Math. Comput. **35**, 773 (1980).
[25] J. Kästner and P. Sherwood, J. Chem. Phys. **128**, 014106 (2008).
[26] A. F. Voter and S. P. Chen, Mater. Res. Soc. Symp. Proc. **82**, 175 (1987).
[27] P. J. Feibelman, Phys. Rev. Lett. **65**, 729 (1990).
[28] L. N. Shchur and M. A. Novotny, Phys. Rev. E **70**, 026703 (2004).
[29] Y. Shim and J. G. Amar, Phys. Rev. B **71**, 115436 (2005).
[30] D. J. Wales, Int. Rev. Phys. Chem. **25**, 237 (2006).
[31] See http://theory.cm.utexas.edu/vtsttools/akmc/ for additional information and the source code for our aKMC scripts.
[32] G. Kresse and J. Hafner, Phys. Rev. B **47**, R558 (1993).
[33] C. R. Henry, Surf. Sci. Rep. **31**, 235 (1998).
[34] G. Haas, A. Menck, H. Brune, J. V. Barth, J. A. Venables, and K. Kern, Phys. Rev. B **61**, 11105 (2000).
[35] L. Xu, G. Henkelman, C. T. Campbell, and H. Jónsson, Phys. Rev. Lett. **95**, 146103 (2005).
[36] G. Barcaro, A. Fortunelli, F. Nita, and R. Ferrando, Phys. Rev. Lett. **95**, 246103 (2005).
[37] L. Xu, G. Henkelman, C. T. Campbell, and H. Jónsson, Surf. Sci. **600**, 1351 (2006).
[38] J. P. Perdew, in *Electronic Structure of Solids*, edited by P. Ziesche and H. Eschrig (Akademie Verlag, Berlin, 1991), p. 11.
[39] D. Vanderbilt, Phys. Rev. B **41**, 7892 (1990).
[40] G. Kresse and J. Joubert, Phys. Rev. B **59**, 1758 (1999).
[41] J. F. Zhu, J. Farmer, N. Ruzycki, L. Xu, C. T. Campbell, and G. Henkelman, J. Am. Chem. Soc. **130**, 2314 (2008).
[42] L. Xu and G. Henkelman, Phys. Rev. B **77**, 205404 (2008).
[43] See http://eon.cm.utexas.edu/ for information about the EON project.